ARTICLES

Interaction of Hydrogen with MOF-5

Silvia Bordiga,[†] Jenny G. Vitillo,[†] Gabriele Ricchiardi,[†] Laura Regli,[†] Donato Cocina,[†] Adriano Zecchina,*[,†] Bjørnar Arstad,[‡,§] Morten Bjørgen,[‡] Jasmina Hafizovic,[‡] and Karl Petter Lillerud[‡]

Dipartimento di Chimica IFM and NIS Centre of Excellence, Via P. Giuria 7, I-10125 Torino, Italy, and Department of Chemistry, University of Oslo, Post Office Box 1033, N-0315 Oslo, Norway

Received: May 18, 2005

Hydrogen storage is among the most demanding challenges in the hydrogen-based energy cycle. One proposed strategy for hydrogen storage is based on physisorption on high surface area solids such as metal−organic frameworks (MOFs). Within this class of materials, MOF-5 has been the first structure studied for hydrogen storage. The IR spectroscopy of adsorbed H_2 performed at 15 K and ab initio calculations show that the adsorptive properties of this material are mainly due to dispersive interactions with the internal wall structure and to weak electrostatic forces associated with $O_{13}Zn_4$ clusters. Calculated and measured binding enthalpies are between 2.26 and 3.5 kJ/mol, in agreement with the H_2 rotational barriers reported in the literature. A minority of binding sites with higher adsorption enthalpy (7.4 kJ/mol) is also observed. These species are probably associated with OH groups on the external surfaces present as termini of the microcrystals.

Introduction

The hydrogen-based energy cycle implies several challenges such as efficient hydrogen production, purification, storage, and conversion. Among these challenges, hydrogen storage is particularly demanding and is considered to be one of the limiting aspects of the technology, especially for mobile applications. So far, a few strategies have been proposed to approach this problem.

One of the most promising strategies is based on the formation of metal hydrides and complex hydrides (alanates, borides, etc.) and involves dissociation of the hydrogen molecule on the surface, followed by penetration into the lattice and formation of chemical bonds with the atoms of the framework.[1] This strategy faces several difficulties including the high cost of some of the metals/alloys, low uptake by weight, and unfavorable adsorption/desorption kinetics (particularly when alanate and boride precursor are considered). A second strategy of considerable importance is based on physisorption on high surface area solids and involves weak dispersion forces and weak polarization effects generated by highly dispersed ionic species. On these materials, a linear correlation between surface area and sorption capacity has been observed.[2] For instance, a high surface area carbon (AC Norit 990293) with BET area of 2029 m^2/g has a sorption capacity at 77 K and 1 bar of 238 mL(STP)/g, corresponding to approximately 2 wt %. Ion-exchanged zeolites[3] are materials where polarization forces associated with the positive counterions dominate. We have recently observed that a promising H_2 uptake can be obtained with proton-exchanged chabazite.[4] H_2 adsorption in hybrid inorganic−organic materials has recently raised considerable interest.[5] Both the inorganic and organic units in these materials could, in principle, offer interactions with hydrogen and contribute to the total uptake. One such material, MOF-5 (also know as IRMOF-1), showing a capacity of 1.13 at 77 K/1 bar,[6] has been investigated with inelastic neutron scattering (INS),[7] obtaining a spectrum showing two main peaks at 10.3 and 12.1 meV assigned to the 0−1 rotational transitions of molecular hydrogen adsorbed on sites I and II, respectively. (See Scheme 1 for sites I and II in MOF-5.)

SCHEME 1

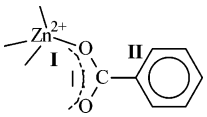

The estimated energy barrier for the rotation of H_2 adsorbed on sites I and II is 1.7 and 1.0 kJ mol^{-1}, respectively, suggesting the occurrence of two interaction sites responsible for the hydrogen uptake. Comparison with calculated rotational barriers for H_2 adsorbed on different sites[8−10] suggests that the corresponding binding energies may be on the same order of magnitude.

IR spectroscopy of adsorbed dihydrogen has proved to be a powerful tool to investigate the perturbation induced on the molecule by surface active sites.[3,4,11] This perturbation is usually accompanied by the onset of IR activity and by a shift of the H−H stretching mode to lower frequency (unperturbed ν(HH) mode appearing at 4161.1 and 4155.2 cm^{-1} for para- and ortho-H_2, respectively[12]). Due to the fact that para-H_2 is the most abundant in the adopted experimental conditions (15 K),

* Corresponding author. E-mail: adriano.zecchina@unito.it.
† Dipartimento di Chimica IFM and NIS Centre of Excellence.
‡ University of Oslo.
§ Present address: Department of Process Technology, SINTEF Materials and Chemistry, N-7465 Trondheim, Norway.

10.1021/jp052611p CCC: $30.25
Published on Web 09/13/2005

normally the shifts are calculated with respect to it. In this paper when not specified we will consider the value of para-H_2 as reference for the unperturbed molecule. Because the frequency shift ($\Delta\nu$) increases with the interaction energy, it is evident that different adsorbing sites can originate distinct IR peaks of adsorbed species. Previously it has been observed that $\Delta\nu$ values are in the range 55−100 cm^{-1} for OH···H_2 interactions in protonic zeolites,[4,13−15] 130−160 cm^{-1} for H_2 perturbed by Lewis sites in zeolites,[15] and 150−230 cm^{-1} for Zn^{2+}···H_2 interactions in ZnH−zeolites.[14]

In this contribution, by combining infrared spectroscopy and high accuracy quantum mechanical calculations, we aimed at clarifying the fundamental aspects of the interactions between H_2 and MOF-5.

Experimental Section

The MOF-5 sample was obtained with a synthesis procedure giving a material with submicrometer-size particles suitable for IR measurements.[16] Prior to the spectroscopic and volumetric measurements, MOF-5 sample has been activated in vacuo at 523 K. The phase purity of the sample has been checked by X-ray diffraction measurements, and the activation procedure has been chosen after control of adsorption properties and sample stability, as described in the Supporting Information. The ZnO sample, with ∼10 m^2/g specific surface area, was obtained by combustion of metallic zinc. ZnO sample has been activated at 673 K to remove all water adsorbed on prismatic faces.[17] The infrared spectra were performed on a prototype instrument developed in our laboratory and described in ref 18 allowing collection of IR spectra in controlled temperature and pressure conditions in the 300−15 K range. Ultrahigh purity hydrogen has been used, and the gas has been passed through a molecular sieve trap immersed in liquid nitrogen before being dosed.

Structure optimizations and single-point calculations have been conducted at the MP2[19] level by means of the Gaussian 98 software package.[20] The basis set used on the H atoms has been 6-311++G**, whereas for the C and O atoms 6-31+G** has been adopted.[21,22] For the Zn atoms an effective core potential (ECP) has been used, whereas the outermost core orbitals have been treated utilizing a double-ζ contraction[23,24] (Lanl2DZ). Single-point calculations on the optimized structures have been done using on the hydrogen atoms the aug-cc-pVQZ[25−27] basis set. The binding energies have all been corrected for the basis set superposition error (BSSE), following the procedure proposed by Boys and Bernardi.[28]

The periodic single-point calculation was done at the BLYP/DN level (GGA functional) with the DMol^3 program[29] (as embedded in Materials Studio 2.2, Accelerys Inc.).[30]

Results and Discussion

Figure 1 reports the IR spectra of MOF-5 as made in air and in vacuum after thermal activation at 523 K, together with the thermogravimetric curve obtained during a ramp to 873 K (inset). Both measurements have been performed on a sample with submicrometer particles, to avoid scattering problems often present when samples with crystals with micrometric dimensions are used. The thermogravimetric measurement indicates that MOF-5 undergoes a consistent weight loss upon thermal treatment in the range 398−523 K, due to H_2O and dimethylformamide (DMF) elimination. At higher temperature, the material does not show any significant weight change up to about 723 K, where the sample starts to decompose.

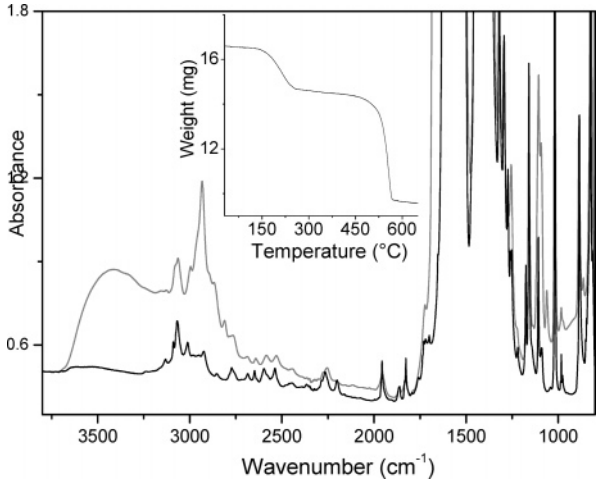

Figure 1. Comparison of MOF-5 IR spectra for as-prepared material (gray curve) and for MOF-5 after activation under high vacuum at 523 K. In the inset a thermogravimetric curve is reported.

The infrared spectrum of an as-prepared MOF-5 (gray curve in Figure 1) can be briefly described in terms of five regions: (i) The first is the 3600−3300 cm^{-1} region, dominated by a broad band centered at 3500 cm^{-1} due to OH groups mainly involved in H-bonds. (ii) The second region is the 3100−2850 cm^{-1} interval, where sharp bands due to aromatic and aliphatic ν(CH) modes of benzene ring and DMF are clearly visible. In this interval, also the first harmonic of the extremely intense ν(CO) vibrations could contribute. (iii) The third region is the 2800−1650 cm^{-1} interval, where many bands due to overtones and combination modes of MOF-5 framework are present. (iv) The fourth region (1650−1300 cm^{-1}) is characterized by very intense bands due to asymmetric and symmetric modes of carboxylate (Raman doublet at 1600 and 1425 cm^{-1}) and by bands due to benzene ring stretching modes and C−H bending vibrations.[31] (v) The fifth region is the 1300−800 cm^{-1} range characterized by skeletal modes. Upon outgassing in vacuo at 523 K, the IR spectrum of MOF-5 (black curve) undergoes substantial changes only in the high-frequency region. In particular, we observe the nearly total disappearance of the broad band centered at 3500 cm^{-1} ascribed to H-bonded ν(OH) groups mainly due to adsorbed water. The very weak broad absorption, still present on the outgassed sample, is explained in terms of ν(OH) of a complex family of hydroxyl groups located on the external surfaces or at internal defects (for instance, 1,4-benzenedicarboxylate vacancies). However, the very weak character of this band ensures that the material under study is characterized by a very low defectivity. Another important feature of the IR spectrum of outgassed MOF-5 is the removal of the doublet at 2941 and 2870 cm^{-1}, associated with ν_{asym} and ν_{sym} of CH_3 species of DMF. Conversely, the band ascribed to the ν(CH) of the aromatic rings (3072 cm^{-1}) is not affected at all, confirming the stability of MOF-5 in the adopted treatment range (see also discussion of Supporting Information).

The activated material corresponding to the lower spectrum of Figure 1 has been cooled to 15 K in the presence of hydrogen. Subsequently, the coverage of the surface was controlled by varying the pressure. Figure 2a reports a series of IR spectra showing the effect of increasing hydrogen coverage on MOF-5 at 15 K. The dashed curve, corresponding to the evacuated MOF-5 spectrum, is characterized by two doublets at 4088−4093 and 4175−4181 cm^{-1}. These bands can be attributed to framework overtones (second harmonic of the extremely intense ν(CO) vibrations and combination modes ν(CC) of benzene ring modes).[31] Upon H_2 adsorption we observe a small perturbation

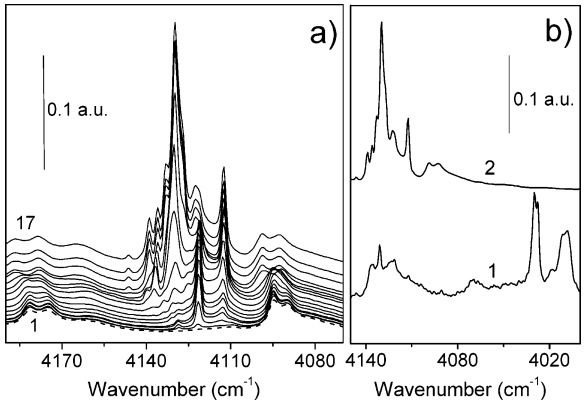

Figure 2. (a) IR spectra of H_2 adsorbed on MOF-5 as a function of gas equilibrium pressure at constant temperature 15 K. Curve 1, $<1 \times 10^{-7}$ bar; curve 17, 0.006 bar. (b) Curve 1, IR spectrum of H_2 adsorbed at 15 K on ZnO sample activated at 673 K. (0.005 bar equilibrium pressure). Curve 2 corresponds to curve 17 of (a) reported for comparison.

of these bands that broaden and blue-shift, and thus suggest that the MOF-5 framework modes slightly respond to hydrogen adsorption. In addition, new sharp components appear in the 4110−4150 cm^{-1} interval. At low H_2 equilibrium coverage ($<1 \times 10^{-7}$−0.003 bar range) a doublet at 4112, 4121 cm^{-1} dominates the IR spectrum. These two narrow bands (full width half-maximum less than 3 cm^{-1}) are separated by about 9 cm^{-1}, i.e. a figure close to that expected for ortho- and para-H_2. For this reason we can hypothesize that they are associated with para- and ortho- H_2 adsorbed on a well-defined family of sites. The corresponding frequency shifts would be −40 and −43 cm^{-1}, respectively. An alternative assignment associates these two peaks with H_2 adsorbed on two slightly different sites. In this case, the frequency shifts would be −49 and −40 cm^{-1}. These small red shifts indicate that the interacting centers have a polarizing power lower than that found for Brønsted sites in zeolites.[4,13−15] By increasing the pressure, a new band at 4130 cm^{-1} grows and gradually becomes the dominant feature. This broader band is characterized by $\Delta\nu = -31$ cm^{-1}, which implies an even lower adsorption energy. The growth of this peak is accompanied by a shift and broadening of the two peaks at 4112 and 4121 cm^{-1}. Satellite bands, likely due to liquefied H_2, appear on the left side and on the right side of the main band when the equilibrium pressure increases up to 0.006 bar (curve 17 in Figure 2a). These satellite peaks are always observed upon low-temperature adsorption of H_2 at surfaces, and their detailed assignment is beyond the scope of this paper.

Another important point to be taken into account when describing the spectroscopic features of Figure 2a is that the extinction coefficient of the doublet at 4112, 4121 cm^{-1} is certainly much higher than that of the component at 4130 cm^{-1} (the extinction coefficient is proportional to the molecular polarization induced by the adsorbing site). This means that the abundance ratio of the sites responsible for the two types of bands is strongly in favor of—about an order of magnitude at least—the less perturbed one at 4130 cm^{-1}. In conclusion, the IR spectroscopy of H_2/MOF-5 system indicates that adsorbed H_2 undergoes sufficient perturbation to make the ν(HH) mode IR active, even if the perturbation is very small. To ascertain if the involved sites are associated with coordinatively unsaturated Zn^{2+} of the $O_{13}Zn_4$ clusters, we compare in Figure 2b the IR spectra of H_2 adsorbed on bulk ZnO.[17] On this material H_2 is reversibly dissociated on Zn−O couples of prismatic faces, giving rise to hydroxyls and Zn hydrides with vibrations at 3500 and 1710 cm^{-1}, repectively.[32] It has been hypothesized that the formation of Zn−H and O−H groups inhibits the reaction of H_2 on the adjacent sites with the result of alternating Zn−O rows remaining empty. Surface Zn^{2+} sites that have not reacted with H_2 and O−H groups present on the virgin surface or formed upon H_2 dissociation can adsorb hydrogen molecularly at higher loadings.[33] Spectrum 1 in Figure 2b corresponds to H_2 adsorbed on ZnO at a loading at which dissociative chemisorption has occurred and further molecular adsorption also takes place. We observe the presence of a doublet at 4029 and 4008 cm^{-1} that is ascribed to H_2 adsorbed on available surface Zn^{2+} ions. Even lower frequency values (different components in the range of 3930−4005 cm^{-1}) have been observed for H_2 adsorbed in Zn-exchanged zeolites.[14] A second group of bands at higher frequencies (4140−4115 cm^{-1}) can be associated with H_2 adsorbed on OH groups formed on Zn^{2+} upon H_2 dissociation. From the comparison of this spectrum with that obtained on MOF-5 (curve 2 in Figure 2b), it can be noted that no bands in the 4040−4000 cm^{-1} region are present in the latter. Moreover, inspection of the O−H and Zn−H spectral regions (not shown in Figure 2) rules out the hypothesis that dissociative chemisorption contributes to hydrogen adsorption in MOF-5. The small red shifts of all the vibrational features of H_2 on MOF-5 indicates that it does not interact directly with exposed Zn^{2+} species. Furthermore, we observe that the doublet at 4112 and 4121 cm^{-1} falls in the region of H_2 adsorbed on OH groups present on the ZnO surface. This suggests assigning it to H_2 interacting with OH groups located on the external surfaces of MOF-5 microcrystals and in local internal defects. The higher polarizing power of these species enhances the intensities of the bands due to H_2 interacting with them, even if the abundance of such species remains low, as can be seen in Figure 1 (black curve). On the basis of the previous discussion, it is inferred that the main component of the IR spectrum of H_2 adsorbed on MOF-5 (band at 4130 cm^{-1}) must be associated with H_2 adsorbed on the walls of the cages.

A more precise evaluation of the interaction energy of the various species can be obtained by isobaric IR experiments. A known pressure of H_2 (0.058 bar) was introduced into the cell, and spectra were then recorded at decreasing temperatures in the range 300−15 K under equilibrium conditions. The intensities of bands at 4112, 4121, and 4130 cm^{-1} have been measured as a function of T. In all cases the intensities increase gradually with decreasing T, reaching asymptotically a maximum at different T values, which corresponds to the saturation of a specific interaction site. The saturation intensity (I_{max}) allows us to know quantitatively, at any T, the fraction of sites covered by H_2, defined as $\theta(T) = I(T)/I_{max}$, and thus the fraction of empty sites $[1 - \theta(T)]$. The equilibrium constant (K_{ads}) of the adsorption process for any given temperature can be described, under the Langmuir approximation, as follows:

$$K_{ads} = \theta(T)/([1 - \theta(T)]P_{CO})$$

Applying the van't Hoff equation, the slope of the $\ln(K_{ads})$ versus $1/T$ gives the adsorption energy. This model, introduced originally by Paukshtis et al.,[34] has more recently been adopted to describe the interaction of H_2 or CO on MgO[11,18] and of H_2 in Li−ZSM-5 by Otero Areán et al.[35] and of H_2 in Na−ZSM-5 by Spoto et al.[36] Figure 3 shows the dependence of $\ln(K_{ads})$ for each species, plotted against $1/T$. We observe a good linear correlation. The slopes give slightly different adsorption enthalpies that range from 7.4 ± 0.2 kJ mol^{-1} for H_2 adsorbed on defects to 3.5 ± 0.1 kJ mol^{-1} for the main site.

In comparison, the adsorption of molecular hydrogen on nanotubes, fibers, and carbons has shown adsorption energies

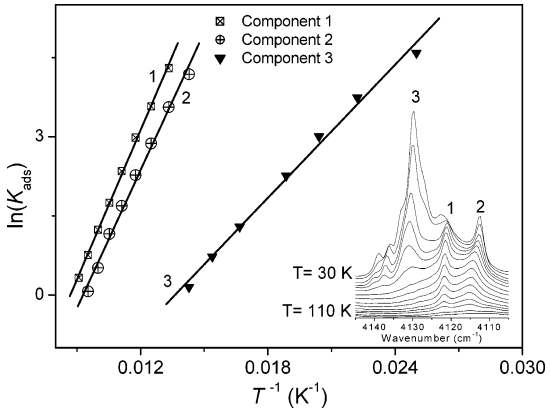

Figure 3. Dependence of ln(K_{ads}), on $1/T$ for H_2 adsorbed on MOF-5 sites labeled "1", "2", and "3" in the inset. Adsorption enthalpies (ΔH) calculated from slope lines are 7.4 ± 0.2 kJ mol^{-1} for sites 1 and 2 and 3.5 ± 0.1 kJ mol^{-1} for site 3. Inset: IR spectra of H_2 adsorbed on MOF-5 as a function of temperature decrease (upper curve 30 K and 0.019 bar equilibrium pressure; lower curve 110 K and 0.035 bar equilibrium pressure).

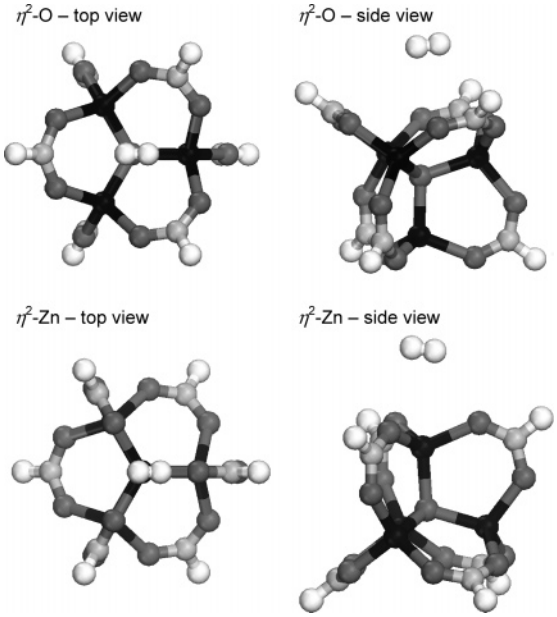

Figure 4. Complexes of $OZn_4(CO_2H)_6$ cluster with hydrogen molecule, in two different interaction geometries resulting from optimization at the MP2 level (see text): η^2-O and η^2-Zn. The elements are coded on a gray scale according to their atomic number: H (white) < C < O < Zn (black).

lower than 5 kJ mol^{-1},[37] while for H_2 interacting with the Brønsted sites in H−SSZ-13 a 9.7 ± 0.3 kJ mol^{-1} enthalpy has been determined.[4] Concerning carbon-based materials, computed interaction energies have been reported by Hübner et al.[8] for the dihydrogen interaction with dilithium terephthalate. The resulting value (4.30 kJ mol^{-1}) was found to be higher than that calculated for a benzene ring (3.63 kJ mol^{-1}) and lower than that estimated for a graphene layer (7.2 kJ mol^{-1}).[38] The higher value calculated for graphene has been attributed to the long-range part of the dispersion forces. For the time being most of the available calculations refer to the interaction of H_2 with organic moieties, while few data have been obtained for the inorganic part. A recent paper[39] has reported a calculated binding energy of 6.86 kJ mol^{-1} for H_2 on the corner of an $OZn_4(CO_2H)_6$ cluster constituted by an oxygen-centered Zn_4O tetrahedron and by six formiate groups. In this work we have adopted the same cluster model but different computational conditions, obtaining slightly different results. Upon optimization, the cluster naturally assumes the structure of the same group of atoms in MOF-5. Indeed, MOF-5 can be described as a cubic arrangement of clusters of this kind, separated by benzene rings.

The interaction of dihydrogen with the O and Zn sites of the Zn_4O unit has been explored, taking into account several different geometries of interaction. Optimization of several starting geometries converged to only two different interaction types, in which the H_2 molecule lies flat on different faces of the inorganic cluster. We will denote these structures as η^2-O and η^2-Zn, according to which cluster atom is closer to the H_2 molecule. However, the interaction of H_2 is not specific with this atom, but in both cases involves all its neighbors. The η^2-O geometry corresponds to the binding site found in ref 39, but with a slight rotation of the hydrogen molecule.

The optimized complexes are shown in Figure 4. The BSSE-corrected binding energy (BE^c) for dihydrogen in η^2-O has been calculated to be 2.26 kJ mol^{-1} in the optimization run and 3.2 kJ mol^{-1} in the single-point calculation with the larger basis set on H atoms. This value is in very good agreement with the experimental value (see above), but it is smaller than the value obtained in ref 39. For η^2-Zn cluster, the BE^c value drops to 0.71 and 2.0 kJ mol^{-1}, respectively. In both cases the dihydrogen is placed side-on with respect to the cluster surface. Concerning the dihydrogen molecule geometry, a slight elongation of the H−H bond is observed upon complexation (0.003 Å in η^2-O and 0.001 Å in η^2-Zn), in accordance with what is expected from the BE^c values. Opposite what we would expect from the BE^c values, the coordination distances of the dihydrogen center from the central coordinating atom are much greater in η^2-O than in η^2-Zn (4.43 versus 3.18 Å). It is worth noticing that in η^2-O the arrangement of the Zn and the carboxylate atoms surrounding the central O atom forms a sort of pocket enclosing the H_2 molecule. The dihydrogen interacts similarly with several atoms. In the η^2-Zn cluster, instead, the Zn atom is well exposed and not shielded by the bonded O atoms. Nevertheless, the number of atoms interacting with the H_2 molecule is lower, reducing the contribution of dispersive forces to the binding energy. The presence of the pocket explains the apparent longer interaction distance observed in the η^2-O cluster. The effect of the electrostatic forces on the interaction has been also qualitatively evaluated by determining the electrostatic potential map based on the experimental structure of MOF-5 reported in ref 40. The electrostatic potential in the solid has been evaluated with a periodic single-point calculation at the BLYP/DN level (GGA functional). The obtained potential surface is shown in Figure 5 (±0.015 au is chosen for the representation of the surface). The electrostatic potential is everywhere positive, except on a torus centered on the Zn atom and formed by the more external oxygen atoms of the cluster. Taking into account the quadrupolar nature of the hydrogen molecule,[41] the map explains on an electrostatic basis the side-on interaction geometry observed for dihydrogen in both clusters. In η^2-O the H_2 molecule is facing a pocket with positive potential, and therefore it is exposed via the negative lobe of its quadrupole (a torus around the bond axis). In η^2-Zn, H_2 exposes its negative lobe to the Zn atom and tilts so that its positive lobe overlaps with the surrounding negative torus.

Nevertheless, the electrostatic potential at the dihydrogen coordination distance is low (about 0.015 au), excluding the presence of strong polarizing centers. In fact, the energetic (BE) and geometric (bond elongation) features of the complexes studied here are similar to those obtained in the gas phase for the interaction of H_2 molecule with the less polarizing K^+ and

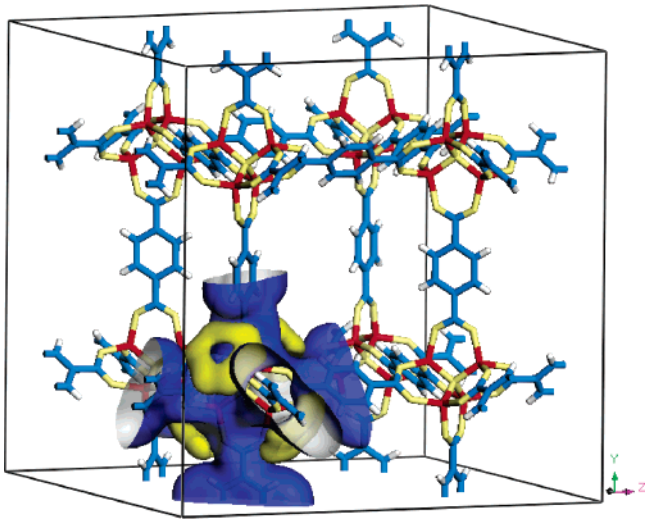

Figure 5. Electrostatic potential map obtained at BLYP/DN level on X-ray resolved structure of MOF-5 reported in ref 40. The isosurfaces corresponding to values of −0.015 and +0.015 au are reported in yellow and blue, respectively. The Zn atoms are reported in red, the H atoms in white, the O atoms in light yellow, and the C atoms in light blue.

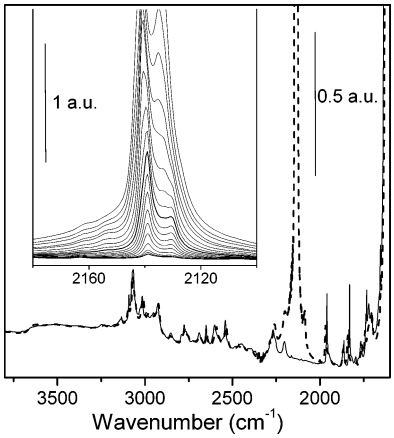

Figure 6. Room-temperature IR spectrum of MOF-5 treated at 473 K under vacuum for 30 min (solid curve); effect of CO adsorbed at 60 K (dashed curve). Inset: Background-subtracted spectra of CO adsorbed on MOF-5 as a function of gas equilibrium pressure at constant temperature of 80 K (upper curve 0.010 bar; lower curve $<1 \times 10^{-7}$ bar).

Rb^+ cations.[42,43] The low interaction energies obtained for dihydrogen adsorbed on $OZn_4(CO_2H)_6$ cluster are of the same order of magnitude of what has been obtained by Hübner et al.[8] for the dihydrogen complexes formed with dilithium terephthalate, which resembles the organic linkers in MOF-5. It seems so evident that for H_2 adsorption on both "inorganic" and/or "organic" parts of MOF-5 the calculated interaction energies exclude the possible presence of strong polarizing centers in MOF-5 at the present level of approximation.

The absence of strong polarizing centers in MOF-5 has been confirmed by CO adsorption at low temperature. The results are reported in Figure 6. Figure 6 reports a general overview of the IR spectrum of MOF-5 in vacuo (solid line) in comparison with that obtained after admission of 0.060 bar of CO and decreasing the temperature at 60 K (CO equilibrium pressure at 60 K is ∼0.003 bar) (dashed line). In this condition, we observe the growth of an extremely intense absorption (out of detectable range) centered at 2136 cm^{-1} and small changes in positions of many absorptions associated with MOF-5 framework vibrations. At 60 K carbon monoxide is entrapped in the porous structure and it desorbs very slowly. To reach more favorable conditions to follow CO desorption, we have increased the temperature up to 80 K. The inset of Figure 6 reports a series of spectra obtained at decreasing CO coverages at 80 K (all the curves are reported after background subtraction). A first general observation is that the spectra profiles are similar to those expected for a hindered rotator,[12] because the presence of the broad rotovibrational tails on both sides of the main component is evident. By reducing the equilibrium pressure the main peak is now resolved in a doublet: 2140 and 2135 cm^{-1}. The component at 2140 cm^{-1} decreases in intensity slowly; conversely the band at 2135 cm^{-1} disappears fast, evidencing a further component at about 2130 cm^{-1}. We assign the band at 2135 cm^{-1} to physisorbed CO, while the components at 2140 and 2130 cm^{-1} are assigned to CO molecules slightly perturbed through the carbon end or through the oxygen end, respectively. The shifts calculated with respect to CO gas are about $|5|$ cm^{-1}. This undoubtedly indicates that the adsorbing matrix does not possess strong polarizing sites and that dispersion forces are mainly involved. This result confirms the data obtained for H_2. Hence we conclude that MOF-5, although not showing any specific interaction site acting as a strong polarizing center (internal surfaces are characterized by very small values of the electrostatic potential at the distance explored by probe molecules), has good adsorptive properties toward H_2. The good adsorbtive properties of MOF-5 are mainly due to dispersion energy forces associated with a specific internal wall topology which is sufficient to ensure a very low H_2 equilibrium pressure at 15 K.

Acknowledgment. We are indebted to Serena Bertarione for kindly supplying unpublished data of H_2 on ZnO and to Carlo Lamberti and Giuseppe Spoto for fruitful discussions. M.B. is grateful for financial support from The Norwegian Research Council through Grant 158552/441. L.R. is grateful for financial support from Regione Piemonte. INSTM Prisma project PRI04RICH is also acknowledged.

Supporting Information Available: Structural characterization of the metal−organic framework under study; volumetric characterization of MOF-5. This material is available free of charge via the Internet at http://pubs.asc.org.

References and Notes

(1) Schlapbach, L.; Züttel, A. *Nature* **2001**, *414*, 353−358.
(2) Nijkamp, M. G.; Raaymakers, J. E. M. J.; van Dillen, A. J.; de Jong, K. P. *Appl. Phys. A* **2001**, *72*, 619−623.
(3) Kazansky, V. B.; Borovkov, V. Y.; Serich, A.; Karge, H. G. *Microporous Mesoporous Mater.* **1998**, *22*, 251−259.
(4) Zecchina, A.; Bordiga, S.; Vitillo, J. G.; Ricchiardi, G.; Lamberti, C.; Spoto, G.; Bjørgen, M.; Lillerud, K. P. *J. Am. Chem. Soc.* **2005**, *127*, 6361−6366.
(5) (a) Li, H.; Eddaoudi, M.; O'Keeffe, M.; Yaghi, O. M. *Nature* **1999**, *402*, 276−279. (b) Rowsell, J. L. C.; Yaghi, O. M. *Angew. Chem., Int. Ed.* **2005**, *44*, 4670−4679. (c)Panella, B.; Hirscher, M. *Adv. Mater.* **2005**, *17*, 538−541.
(6) Rowsell, J. L. C.; Millward, A. R.; Park, K. S.; Yaghi, O. M. *J. Am. Chem. Soc.* **2004**, *126*, 5666−5667.
(7) Rosi, N. L.; Eckert, J.; Eddaoudi, M., Vodak, D. T.; Kim, J.; O'Keeffe, M.; Yaghi, O. M. *Science* **2003**, *300*, 1127−1129.
(8) Hübner, O.; Glöss, A.; Fichtner, M.; Klopper, W. *J. Phys. Chem. A* **2004**, *108*, 3019−3023.
(9) Vitillo, J. G.; Damin, A.; Zecchina, A.; Ricchiardi, G. *J. Chem. Phys.* **2005**, *122*, 114311.
(10) Hamel, S.; Côté, M. *J. Chem. Phys.* **2004**, *121*, 12618−12625.
(11) Gribov, E. N.; Bertarione, S.; Scarano, D.; Lamberti, C.; Spoto, G.; Zecchina, A. *J. Phys. Chem. B* **2004**, *108*, 16174−16186.
(12) Zecchina, A.; Otero Areán, C.; Turnes Palomino, G.; Geobaldo, F.; Lamberti, C.; Spoto, G.; Bordiga, S. *Phys. Chem. Chem. Phys.* **1999**, *1*, 1649−1657.

(13) Makarova, M. A.; Zholobenko, V. L.; Al-Ghfaili, K. M.; Thompson, N. E.; Dewing, J.; Dwyer, J. *J. Chem. Soc., Faraday Trans.* **1994**, *90*, 1047−1054.

(14) Kazansky, V. B.; Serykh, A. I.; Anderson, B. G.; Van Santen, R. A. *Catal. Lett.* **2003**, *88*, 211−217.

(15) Zecchina, A.; Spoto, G.; Bordiga, S. *Phys. Chem. Chem. Phys.* **2005**, *7*, 1627−1642.

(16) Huang, L.; Wang, H.; Chen, J.; Wang, Z.; Sun, J.; Zhao, D.; Yan, Y. *Microporous Mesoporous Mater.* **2003**, *58*, 105−114.

(17) Scarano, D.; Spoto, G.; Bordiga, S.; Zecchina, A.; Lamberti, C. *Surf. Sci.* **1992**, *276*, 281−298.

(18) Spoto, G.; Gribov, E. N.; Ricchiardi, G.; Damin, A.; Scarano, D.; Bordiga, S.; Lamberti, C.; Zecchina, A. *Prog. Surf. Sci.* **2004**, *76*, 71−146.

(19) Møller, C.; Plesset, M. S. *Phys. Rev.* **1934**, *46*, 618−622.

(20) Frisch, M. J.; Trucks, G. W.; Schlegel, H. B.; Scuseria, G. E.; Robb, M. A.; Cheeseman, J. R.; Zakrzewski, V. G.; Montgomery, J. A., Jr.; Stratmann, R. E.; Burant, J. C.; Dapprich, S.; Millam, J. M.; Daniels, A. D.; Kudin, K. N.; Strain, M. C.; Farkas, O.; Tomasi, J.; Barone, V.; Cossi, M.; Cammi, R.; Mennucci, B.; Pomelli, C.; Adamo, C.; Clifford, S.; Ochterski, J.; Petersson, G. A.; Ayala, P. Y.; Cui, Q.; Morokuma, K.; Salvador, P.; Dannenberg, J. J.; Malick, D. K.; Rabuck, A. D.; Raghavachari, K.; Foresman, J. B.; Cioslowski, J.; Ortiz, J. V.; Baboul, A. G.; Stefanov, B. B.; Liu, G.; Liashenko, A.; Piskorz, P.; Komaromi, I.; Gomperts, R.; Martin, R. L.; Fox, D. J.; Keith, T.; Al-Laham, M. A.; Peng, C. Y.; Nanayakkara, A.; Challacombe, M.; Gill, P. M. W.; Johnson, B.; Chen, W.; Wong, M. W.; Andres, J. L.; Gonzalez, C.; Head-Gordon, M.; Replogle, E. S.; Pople, J. A. *Gaussian 98*, Revision A.11; Gaussian, Inc.: Pittsburgh, PA, 2001.

(21) Hehre, W. J.; Radom, L.; Schleyer, P. v. R.; Pople, J. A. *Ab Initio Molecular Orbital Theory*; John Wiley & Sons Inc.: New York, 1986.

(22) Frisch, M. J.; Pople, J. A.; Binkley, J. S. *J. Chem. Phys.* **1984**, *80*, 3265−3269.

(23) Hay, P. J.; Wadt, W. R. *J. Chem. Phys.* **1985**, *82*, 270−283.

(24) Wadt, W. R.; Hay, P. J. *J. Chem. Phys.* **1985**, *82*, 284−298.

(25) Dunning, T. H., Jr. *J. Chem. Phys.* **1989**, *90*, 1007−1023.

(26) Peterson, K. A.; Woon, D. E.; Dunning, T. H. *J. Chem. Phys.* **1994**, *100*, 7410−7415.

(27) Kendall, R. A.; Dunning, T. H.; Harrison, R. J. *J. Chem. Phys.* **1992**, *96*, 6796−6806.

(28) Boys, S. B.; Bernardi, F. *Mol. Phys.* **1970**, *19*, 553−559.

(29) Delley, B. *J. Chem. Phys.* **1990**, *92*, 508−517.

(30) *Materials Studio 2.2*, Discover module; Accelrys Inc.: San Diego, CA, 2002.

(31) Bordiga, S.; Lamberti, C.; Ricchiardi, G.; Regli, L.; Bonino, F.; Damin, A.; Lillerud, K.-P.; Bjørgen, M.; Zecchina, A. *Chem. Commun.* **2004**, 2300−2301.

(32) Boccuzzi, F.; Borello, E.; Zecchina, A.; Bossi, A.; Camia, M. *J. Catal.* **1978**, *51*, 150−159.

(33) Zecchina, A.; Scarano, D.; Bordiga, S.; Spoto, G.; Lamberti, C. *Adv. Catal.* **2001**, *46*, 265−397.

(34) Paukshtis, E. A.; Yurchenko, N. E. *Russ. Chem. Rev.* **1983**, *52*, 426−454.

(35) Otero Areán, C.; Manilova, O. V.; Bonelli, B.; Rodríguez Delgado, M.; Turnes Palomino, G.; Garrone, E. *Chem. Phys. Lett.* **2003**, *370*, 631−635.

(36) Spoto, G.; Gribov, E.; Bordiga, S.; Lamberti, C.; Ricchiardi, G.; Scarano, D.; Zecchina, A. *Chem. Commun.* **2004**, 2768−2769.

(37) Schimmel, H. G.; Kearley, G. J.; Nijkamp, M. G.; Visser, C. T.; de Jong, K. P.; Mulder, F. M. *Chem Eur. J.* **2003**, *9*, 4764−4770.

(38) Heine, T.; Zhechkov, L.; Seifert, G. *Phys. Chem. Chem. Phys.* **2004**, *6*, 980−984.

(39) Sagara, T.; Klassen, J.; Ganz, E. *J. Chem. Phys.* **2004**, *121*, 12543−12547.

(40) Eddaoudi, M.; Kim, J.; Rosi, N.; Vodak, D.; Wachter, J.; O'Keefe, M.; Yaghi, O. M. *Science* **2002**, *295*, 469−472.

(41) Garrone, E.; Kazansky, V. B.; Kustov, L. M.; Sauer, J.; Senchenya, I. N.; Ugliengo, P. *J. Phys. Chem.* **1992**, *96*, 1040−1045.

(42) Bushnell, J. E.; Kemper, P. R.; Bowers, M. T. *J. Phys. Chem.* **1994**, *98*, 2044−2049.

(43) Barbatti, M.; Jalbert, G.; Nascimento, M. A. C. *J. Chem. Phys.* **2001**, *114*, 2213−2218.